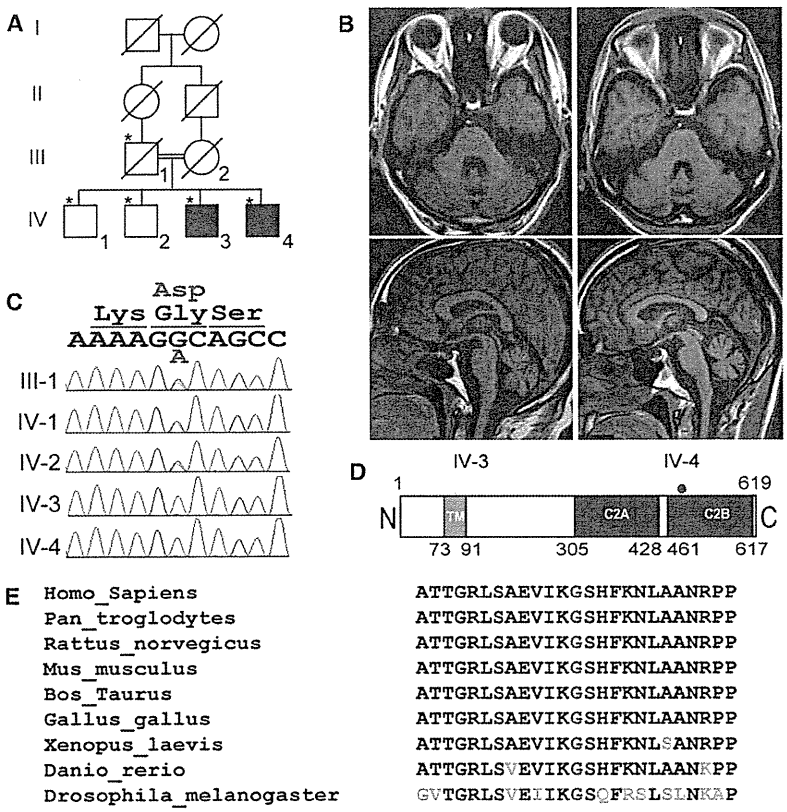

Figure 1. Familial Pedigree, Brain MRI of Patients, and the *SYT14* Mutation Identified
(A) Familial pedigree of the patients with autosomal-recessive spinocerebellar ataxia. *An asterisk indicates members whose genomic DNA was available for this study.
(B) Brain MRI of IV-3 at 59 years of age (left panels) and IV-4 at 56 years of age (right panels). Axial (upper panels) and sagittal (lower panels) sections of a T1-weighted image are shown.
(C) Electropherograms of unaffected (III-1, IV-1, and IV-2) and affected (IV-3 and IV-4) members, who show the mutation.
(D) Schematic presentation of SYT14. The red dot indicates the location of the mutation in the C2B domain.
(E) The missense mutation occurred at an evolutionarily conserved amino acid (in red).

movements were observed. Laboratory examination, including analysis of serum albumin, vitamin E, and α-fetoprotein, was normal. A nerve-conduction study (NCS) indicated no neuropathy. No retinitis pigmentosa was recognized by ophthalmologic evaluation. Brain magnetic resonance imaging (MRI) revealed mild atrophy of the cerebellar vermis and hemispheres but no apparent atrophy of the brain stem or the cerebral cortex. (Figure 1B, left panels).

Similar to IV-3, IV-4 also had psychomotor retardation from childhood, but this retardation was more severe than that of IV-3. After graduation from a school for disabled children at the age of 15, he entered a facility for disabled people. He showed gait disorder, but he was able to walk without a cane. At an age of ~50, his gait disturbance worsened, and he went for a medical check at a hospital when he was 56 years old. He displayed disturbance of smooth-pursuit eye movements, gaze-evoked horizontal nystagmus, dysarthria, mild limb ataxia, and moderate truncal ataxia. No involuntary movements were observed. His laboratory tests, including those for serum albumin, vitamin E, and α-fetoprotein, were normal. NCS was normal. A brain MRI was similar to that of IV-3 (Figure 1B, right panels). The clinical manifestations of these two patients are summarized in Table 1.

To search for the disease locus, we conducted genome-wide SNP genotyping of III-1, IV-1, IV-2, IV-3, and IV-4 by using the Genome-wide Human SNP Array 6.0 (SNP 6.0 array) (Affymetrix, Inc., Santa Clara, CA) according to the manufacturer's instructions. Then, SNP 6.0 array data were subjected to homozygosity mapping with HomozygosityMapper software.[7] For the linkage analysis, a subset of 7339 SNPs with high heterozygosity (mean heterozygosity 0.49) was extracted from the SNP 6.0 array data with the program Linkdatagen, for which the bin size was set to 0.5cM and the allele frequency of the Japanese population was used.[8] The multipoint LOD score was calculated with Allegro version 2[9] on the basis of the model of autosomal-recessive and X-linked-recessive inheritance, respectively. In both models, complete penetrance and a disease-allele frequency of 0.0001 were adopted. The homozygosity mapping revealed a total of three regions, which together were approximately 11.35 Mb in size, as candidate loci, where genes known to be mutated in ARCA did not exist (Table 2). In the model of autosomal-recessive inheritance, a total of ten regions with a LOD score greater than 1.5 in the multipoint linkage analysis were identified (Table S1). The three homozygous regions in accordance with the linked regions still survived as candidate regions. On the basis of X-linked recessive inheritance, a total of three regions with positive LOD scores (maximum LOD score = 0.9031) were highlighted; together, these three regions were approximately 101.03 Mb (Table S1).

To find a gene mutation within the candidate loci, we performed whole-exome sequencing on IV-3 and IV-4. Three micrograms of genomic DNA was processed with the SureSelect Human All Exon Kit v.1 (approximately 180,000 exons covering 38 Mb of the CCDS database) (Agilent Technologies, Santa Clara, CA) according to the manufacturer's instructions. Captured DNAs were sequenced on an Illumina GAIIx (Illumina, San Diego, CA) with 76 bp pair-end reads. Of the possible eight lanes of the flow cell, two lanes for IV-3 and three lanes for IV-4 (Illumina) were used. Image analysis and base calling

Table 1. Clinical Features of the Patients

Clinical Features	IV-3	IV-4
Age at present	61	58
Sex	male	male
Age of obvious ataxia	56	around 50
Mental retardation	mild	moderate
Ocular apraxia	no	no
Ophthalmoplegia	no	no
Nystagmus	no	+
Dysarthria	+	+
Truncal ataxia	++	++
Limb ataxia	+	+
Extrapyramidal signs	no	no
Involuntary movements	no	no
Sensory involvements	no	no
Tendon reflex	normal-increased	normal-decreased
Plantar responses	normal	normal
Peripheral neuropathy	no	no
Pes cavus	no	no
SARA[a]	12/40	15/40
Cerebellar atrophy on MRI	+	+
others	normal level of serum albumin, vitamin E, and α-fetoprotein	normal level of serum albumin, vitamin E, and α-fetoprotein

[a] SARA: Scale for the assessment and rating of ataxia.[32]

Table 2. Regions of Homozygosity

Chromosome	Chromosomal Position (rsID)	Size (Mb)	LOD
1	207226930 (rs2761781)–213992561 (rs1857229)	6.77	2.0537
4	181929079 (rs918401)–185188999 (rs7690914)	3.26	2.0554
22	45676443 (rs3905396)–47003473 (rs2013591)	1.33	2.0545

Regions of homozygosity were identified by HomozygosityMapper, and the LOD scores were calculated by multipoint linkage analysis, for which SNPs were extracted from SNP 6.0 array data via Linkdatagen.

were performed by sequence control software (SCS) real-time analysis (Illumina) and CASAVA software v1.6 (Illumina). Reads were aligned to the human reference genome sequence (UCSC hg18, NCBI build 36.1) via the ELAND v2 program (Illumina). Coverage was calculated statistically with a script created by BITS (Tokyo, Japan). Approximately 71 million reads from IV-3 and 148 million reads from IV-4 (these numbers of reads passed quality-control [Path Filter]) were mapped to the human reference genome with Mapping and Assembly with Qualities (MAQ)[10] and NextGENe software v2.00 (SoftGenetics, State College, PA) under the default settings. MAQ aligned 59,491,138 and 126,159,746 reads to the whole genome for IV-3 and IV-4, respectively. A script created by BITS was used for extraction of SNPs and indels from the alignment data; dbSNP build 130 served as a reference for registered SNPs. A consensus quality score of 40 or more was adopted for the SNP analysis in MAQ. Coverage analysis revealed that 65.0% (IV-3) and 71.3% (IV-4) of the coding sequences (CDS) were completely covered (100%), and 77.7% (IV-3) and 80.3% (IV-4) of CDS were mostly covered by reads (90% or more) through the whole genome. 79.0% (IV-3) and 79.7% (IV-4) of total CDS were covered by ten reads or more (50 reads or more in 66.4% and 77.1%, respectively).

To identify the pathogenic mutation, we adopted a prioritization scheme, which has been used in recent studies.[11–13] First, we excluded the variants registered in dbSNP130 from all the detected variants and then picked up homozygous mutations and variants in coding regions and the intronic regions within 50 bp from coding sequences. Of the homozygous mutations and variants, we focused on those within the candidate regions. As a result, only two missense mutations or variants, p.Gly484Asp (c.1451G>A) (NM_001146261.1) in exon 8 of *SYT14* (1q32.2, [MIM 610949]) and p.Gln4203Arg (c.12608A>G) (NM_206933.2) in exon 63 of *USH2A* (1q41, [MIM 608400]) remained as candidates for both cases (Table S2). Sanger sequencing with ABI 3500xL (Life Technologies, Carlsbad, CA) confirmed that the c.1451G>A of *SYT14* was homozygous in IV-3 and IV-4 and heterozygous in III-1 (father), IV-1, and IV-2, whereas the c.12608A>G of *USH2A* was homozygous in IV-2 as well as IV-3 and IV-4 (Figure 1C and data not shown). The *SYT14* missense mutation occurred at an evolutionarily conserved amino acid among different species and resides in the second C2 (C2B) domain (Figures 1D and 1E). In silico analysis incorporating different tools, including Polyphen, Polyphen2, SIFT, and Align GVGD, consistently indicated that the change was damaging (Table S3). The mutation was not detected in 576 Japanese control chromosomes, indicating that the mutation is very rare. On the basis of the X-linked recessive model, no pathological hemizygous mutation of protein-coding genes was detected in the possible candidate loci (Table S4).

We considered the *SYT14* mutation to be the causative agent and used the Sanger method to conduct mutation screening of all the coding regions of *SYT14* in 65 simplex SCA cases and 37 SCA familial cases, including three with autosomal-recessive inheritance. Only p.Gly183Glu (c.548G>A) was found in one family with autosomal-dominant SCA; however, the change was not consistent with the SCA phenotype in the family (Table S3). Thus, we could not detect any other pathological changes in *SYT14*. This was probably due to the small number of cases tested.

Synaptotagmin XIV (SYT14), which is encoded by *SYT14*, is a member of the synaptotagmins (SYTs), which are membrane-trafficking proteins, and SYT14 is conserved across many organisms.[14] Although the original report indicated that *SYT14* was not expressed in mouse brain,[14] multiple lines of evidence, including from the Allen brain Atlas, suggest that *SYT14* is expressed in the central nervous system (CNS) of the fly, mouse, and human brains.[15,16] To confirm *SYT14* expression in the CNS, we performed TaqMan quantitative real-time PCR analysis with cDNAs of adult human tissue (Human MTC Panel I, #636742) (Clontech Laboratories, Mountain View, CA), fetal human tissue (Human Fetal MTC Panel, #636747) (Clontech Laboratories), mouse tissue (Mouse MTC Panel I, #636745) (Clontech Laboratories), and various regions of the mouse brain (GSMBRSET) (NIPPON Genetics, Tokyo, Japan) as templates. Predesigned TaqMan probe sets for human *SYT14* (Hs00950169_m1), mouse *Syt14* (Mm00805319_m1), human *β-actin* (*ACTB*, 4326315E), and mouse *Actb* (43522341E) from Applied Biosystems were used. PCR reactions (total volume of 20 μl) contained 10 μl of the TaqMan Gene Expression Master Mix (Applied Biosystems), 1 μl of 20 × TaqMan reagents for *ACTB/Actb* and *SYT14/Syt14*, and 1 μl of cDNA (containing 1 ng cDNA in MTC panels and 25 ng cDNA in GSMBRSET) as the template. PCR was performed on a Rotor-Gene Q (QIAGEN, Valencia, CA) as follows: 2 min at 50°C and 10 min at 95°C, then 40 cycles of 95°C for 15 s and 60°C for 1 min. Expression levels were calculated with the Rotor-Gene Q Series Software (QIAGEN) by the $2^{-\Delta\Delta Ct}$ method. The cycling threshold (Ct) of the target gene was compared with the Ct of *ACTB* cDNA, and ΔCt was expressed as Ct of *SYT14* − Ct of *ACTB*. ΔΔCt was expressed as ΔCt of the control sample − ΔCt of each sample, and relative concentration was determined as $2^{-\Delta\Delta Ct}$. Expression in the kidney and the cerebral cortex was used as the control in Figures 2A–2D. *SYT14* was predominantly expressed in human adult and fetal brain tissues (Figures 2A and 2B). Even in mice, substantial expression in the brain was confirmed (but, not predominant) (Figure 2C). Among various brain regions in mice, *SYT14* was mostly expressed in the cerebellum (Figure 2D).

Intracellular distribution of SYT14 in cultured cells was investigated. The full-length *SYT14* PCR product amplified from human brain cDNA (MHS4426-99239810, Open Biosystems, Huntsville, AL) was used as a template and subcloned into pDONR221 (the entry vector of Gateway system, Invitrogen). We used site-directed mutagenesis to produce the *SYT14* mutant and variants by using a mutagenesis kit (Toyobo, Osaka, Japan). Variants include c.611C>T and c.810_812del, which are registered in dbSNP130, and c.548G>A, which was detected in an SCA patient with autosomal-dominant inheritance but did not segregate with the phenotype, indicating that it is nonpathogenic (Table S3). All constructs were verified by DNA sequencing. Each construct was recloned into the pEF-DEST51 mammalian expression vector (Invitrogen) and transfected to COS-1 cells with the FuGENE^{R}6 transfection reagent (Roche Applied Science, Mannheim, Germany) according to the manufacturer's instructions. Localization of the mutant (p.Gly484Asp) was clearly different from that of the wild-type and other (normal) variants. Whereas the wild-type and other variants were localized to the perinuclear and submembranous regions, p.Gly484Asp was localized in the cytoplasm (significant amounts were in the perinuclear region) but formed a characteristic reticular pattern without showing any submembranous distribution (Figures 2E and S2B). Confocal microscopic analysis showed that the p.Gly484Asp mutant was colocalized with an endoplasmic reticulum (ER) marker, protein disulfide isomerase (PDI), throughout the cells, whereas the wild-type colocalized with PDI dominantly in perinuclear regions (Figure 2F). immunoblot analysis combined with subcellular fractionation of the transfected cells further confirmed that the mutant was distributed differently from the wild-type. The wild-type and the mutant (p.Gly484Asp) were distributed in the nucleus and Golgi apparatus fractions; however, only the mutant was detected in microsome fractions containing ER fragments together with an ER membrane marker, calnexin (Figure S1).[17] These data suggest that improper folding of the mutant protein results in abnormal retention in the ER.

To investigate the effect of the p.Gly484Asp mutation in the C2B domain on phospholipid binding activity, we amplified cDNA of C2B domains from the wild-type and the p.Gly484Asp mutant from SYT14-expressing vectors by using the following primers: sense, 5′-GGATCCGAAA GTACATCCTCATGTCA-3′; and antisense, 5′-TCATGAC TCTAGCAACGCAT-3′. We then recloned the cDNA into *Escherichia coli* (*E. coli*) expressing vector (pGEX-4T-3). The C2B domain of SYT14 fused to glutathione S-transferase (GST) was expressed in *E. coli* JM109 and purified by standard protocols. Both GST-SYT14-C2B (WT) and GST-SYT14-C2B (p.Gly484Asp) could be mostly purified of contamination by degradation products, but the amount of GST-SYT14-C2B (p.Gly484Asp) obtained was at least four times smaller than that of GST-SYT14-C2B (WT) (data not shown). Liposome (phosphatidylcholine and phosphatidylserine, 1:1, w/w) cosedimentation assay with purified GST-SYT14-C2B was performed as described previously.[18] The result showed that the SYT14-C2B (p.Gly484Asp) bound liposomes similarly to SYT14-C2B (WT) (Figure 2G), indicating that the p.Gly484Asp mutation had no effect on the Ca^{2+}-independent phospholipid-binding activity of the SYT14-C2B domain.

The Allen Mouse Brain Atlas indicates that *Syt14* is expressed in Purkinje cells of the cerebellum in mice; however, SYT14 localization has not been fully investigated.[15] A rabbit polyclonal anti-SYT14 antibody (Ab-SYT14) was generated for immunoblotting and immunocytochemistry (Operon Biotechnologies, Tokyo, Japan) (Figure S2). Immunohistochemical analysis of mouse and human brains was

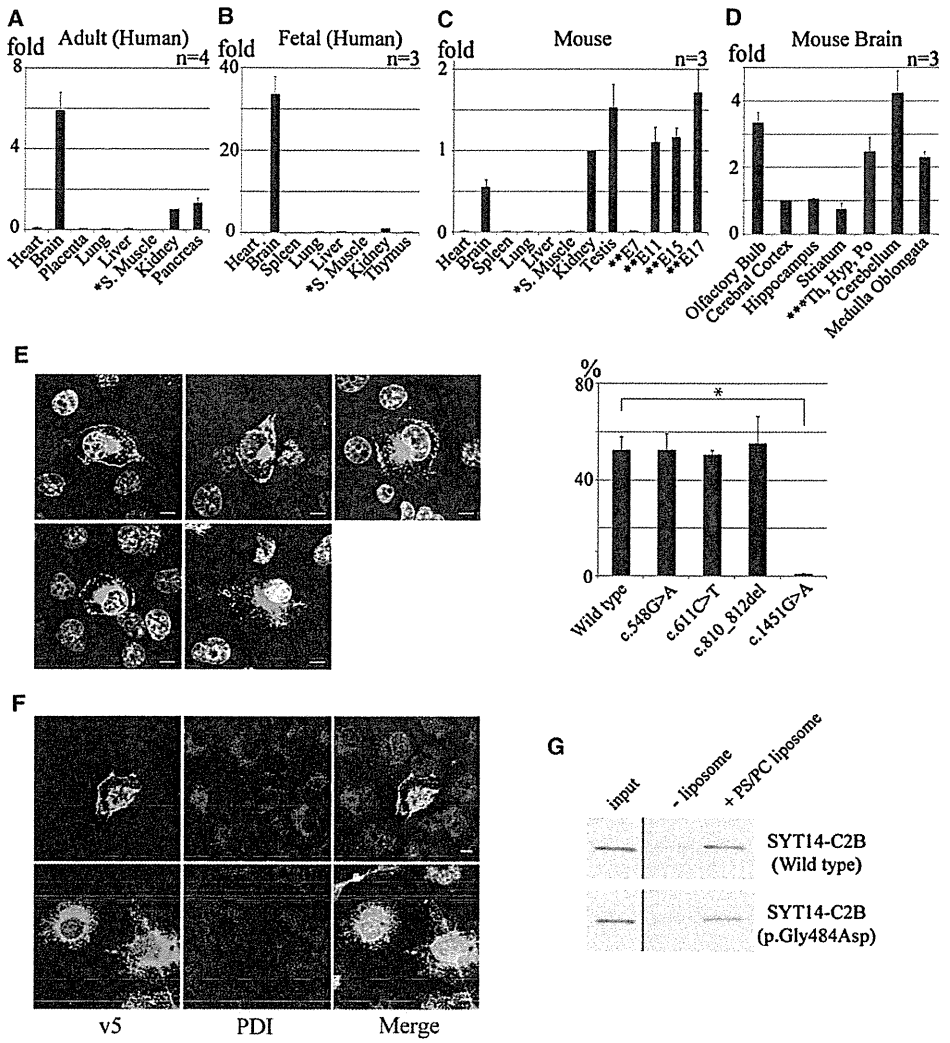

Figure 2. Expression Studies of *SYT14/Syt14* cDNA in Human and Mouse Tissues and Localization of SYT14 in Transfected COS-1 Cells
(A–D) The results of a TaqMan quantitative real-time PCR assay in which the first-strand cDNA of human adult tissues (A), human fetal tissues (B), mouse tissues (C), and various regions of mouse brain (D) were used as templates. The relative cDNA concentrations were determined from cDNA concentrations of the kidney (human adult tissues, human fetal tissues, and mouse tissues) or cerebral cortex (various regions of the mouse brain). Error bars represent the standard deviation. *S. Muscle indicates skeletal muscle. **E7, **E11, **E15, and **E17 indicate mouse embryos at 7, 11, 15, and 17 days of embryonic development, respectively. ***Th, Hyp and Po indicate thalamus, hypothalamus, and pons.
(E) Immunocytochemistry of COS-1 cells transfected with expression vectors of v5/His-tagged wild-type (upper left), p.Gly183Glu (c.548G>A) (upper middle), p.Pro203Leu (c.611C>T) (upper right), p.Glu270del (c.810_812del) (lower left), or p.Gly484Asp (c.1451G>A) (lower middle) SYT14. The SYT14 was detected with the anti-v5 antibody (Alexa fluor 488 as the secondary antibody). Nuclei were stained (white) with 4′,6-diamidino-2-phenylindole (DAPI). The horizontal bars indicate 10 μm. The bar graph indicates the ratio of the cells in which overexpressed proteins were accumulated in submembranous regions. A total of 120 cells per each transfectant in triplicated experiments were counted. Submembranous localization of the mutant (p.Gly484Asp) was mostly unseen, in contrast to the wild-type (*$p < 0.001$).
(F) Immunocytochemical analysis of COS-1 cells transfected with expression vectors of v5/His-tagged wild-type (upper panels) or the p.Gly484Asp mutant (lower panels). The SYT14 was detected with the anti-v5 antibody (Alexa fluor 488 as the secondary antibody), and PDI (protein disulfide isomerase) was visualized with an anti-PDI antibody (Alexa fluor 546 as the secondary antibody). Nuclei were stained (white) with DAPI. The scale bar represents 10 μm. The anti-v5 and anti-PDI antibodies and the Alexa-488-conjugated secondary antibody were all used at a dilution of 1:1000.
(G) Phospholipid binding activity of the C2B domain of the wild-type SYT14 and the p.Gly484Asp mutant. Liposomes and GST-fusion proteins (2 μg) were incubated in 50 mM HEPES-KOH (pH 7.2) in the presence of 2 mM EGTA for 15 min at room temperature. After centrifugation at 12,000 × *g* for 10 min, the supernatants (non-binding fraction) and pellets (phospholipid-binding fraction) were separated as described previously.[18] The pelleted samples and input samples (100 ng) were subjected to 10% SDS-PAGE followed by immunoblotting with horseradish peroxidase-conjugated anti-GST antibody (Santa Cruz Biotechnology, Santa Cruz, CA).

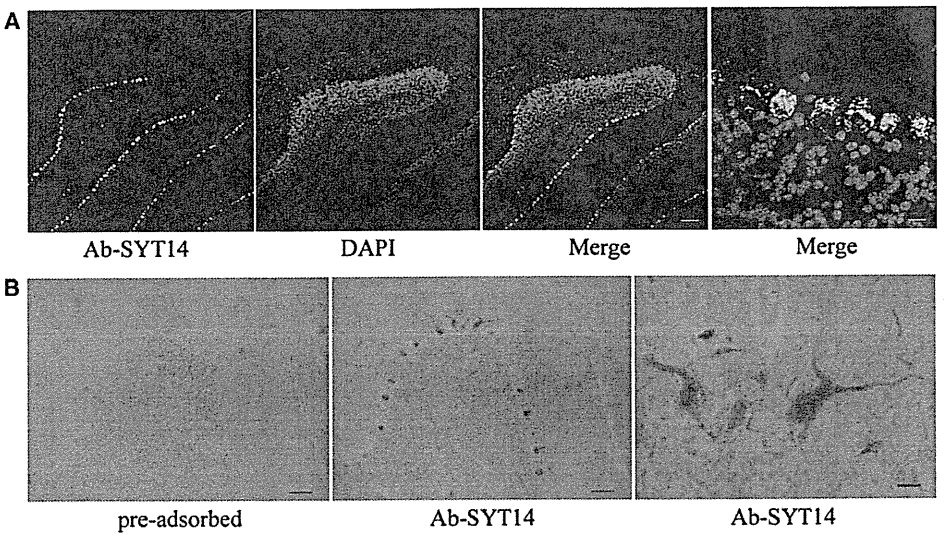

Figure 3. Selective Localization of SYT14 in Purkinje Cells of the Cerebellum in Mice and Humans
(A) Immunohistochemical analysis with the Ab-SYT14 antibody of the cerebellum from an adult mouse at 12 weeks of age. Nuclei were stained with DAPI (the scale bar represents 100 μm). A magnified image is shown in the first right panel (the scale bar represents 10 μm).The Ab-SYT14 antibody (0.9 mg/dl) was used at a dilution ration of 1:2000, and the Alexa-488-conjugated secondary antibody dilution was 1:1000.
(B) Immunohistochemical analysis with the Ab-SYT14 antibody of the cerebellum from the human control. Ab-SYT14 antibodies were preincubated with (left panel) or without (middle panel) peptide antigen before immunostaining. Nuclei were stained with hematoxylin (scale bars represent 100 μm). A magnified image is shown in the right panel (the scale bar represents 20 μm). The Ab-SYT14 antibody (0.9 mg/dl) was used at a dilution of 1:500.

performed with Ab-SYT14, as previously described.[19–21] Mouse brain sections were prepared at the RIKEN Brain Science Institute. Mouse experimental protocols were approved by the animal experiment committee of the RIKEN Brain Science Institute. The frozen brain of C57BL/6J mouse was mounted in Tissue-Tek and sliced to 10 μm sections with a freezing microtome. A human adult brain specimen was obtained through the postmortem examination of a brain from a control subject without neurodegenerative disorders. Informed consent was obtained from the family on the basis of the IRB-approved protocol of Yokohama City University School of Medicine. The human brain was fixed in 10% formalin and cut into 1-cm-thick slices. Sliced tissues were embedded in paraffin wax, and 5 μm sections were immunostained with primary antibodies and visualized with the Vectastain ABC kit (Vector Laboratories, Burlingame, CA). Selective localization of SYT14/Syt14 in Purkinje cells of the mouse cerebellum (Figure 3A) and human cerebellum (Figure 3B) were recognized, indicating that SYT14 plays an important role in the cerebellum. These data are in agreement with a scenario in which the *SYT14* mutation causes cerebellar degeneration in this family.

In this study, only one p.Gly484Asp mutation of *SYT14* was identified in association with SCA. Quintero-Rivera et al.[16] previously described a 12-year-old female with cerebral atrophy, absence seizures, developmental delay with a WISC III score of 58 for full IQ, and de novo t(1;3)(q32.1;q25.1) disrupting *SYT14*. Her brain MRI showed diffuse cerebral atrophy, including that of the cerebellar hemisphere and vermis. Although the inheritance modes are different (recessive impact on our family and dominant on the female patient), mild to moderate mental retardation and cerebellar atrophy are common among patients with *SYT14* abnormalities. It will be important to assess the future phenotype of the female patient studied by Quintero-Rivera et al.[16]

Relatively common ARCAs in Japan include ataxia, early-onset; oculomotor apraxia, hypoalbuminemia/ataxia-oculomotor apraxia 1 (EAOH/AOA1 [MIM 208920]); ataxia-oculomotor apraxia 2 (AOA2 [MIM 606002]); spastic ataxia; Charlevoix-Saguenay type (SACS [MIM 270550]); ataxia with isolated vitamin E deficiency (AVED [MIM 277460]); and ataxia-telangiectasia (AT [MIM 208900]). (Friedrich ataxia 1 [FRDA (MIM 229300)] has never been described in the Japanese population.) In this family, patients never showed ocularmotor apraxia, spasticity, peripheral neuropathy, retinal abnormality, immunological abnormality, or other systemic involvements. As an adult-onset type of pure ARCA, SYNE1-related ARCA (also known as spinocerebellar ataxia, autosomal-recessive 8; SCAR8 [MIM 610743]) is found to be caused by mutations of the gene encoding synaptic nuclear envelope protein 1.[22] Furthermore, these patients were not associated with psychomotor retardation. Thus, SYT14-mutated ARCA, described here, should be categorized to a distinct type of ARCA.

SYTs is a large family of transmembrane proteins associated with exocytosis of secretory vesicles (including synaptic vesicles).[23] The mammalian SYT family is composed

of 17 members. SYTs are anchored to the secretory vesicles via a single transmembrane domain (TM) close to its N terminus and have tandem cytoplasmic domains, C2A and C2B.[24] Among SYTs, SYT1 (MIM 185605) is involved in neurotransmitter release and has been intensively studied. The crystal structure of the C2 domains consists of a compact eight-stranded β-barrel with two protruding loops (loops 1 and 3) that form the Ca^{2+}-binding pockets.[25] SYT1 binds three and two Ca^{2+} ions via loops 1 and 3 of C2A and C2B, respectively. Ca^{2+} binding triggers the rapid penetration of the C2 domains into membranes harboring negatively charged phospholipids. Ca^{2+} also promotes SYT1 binding to t-SNAREs (target-membrane-soluble N-ethylmaleimide-sensitive factor attachment protein receptors). SYT1 is a key sensor for evoked and synchronous neurotransmitter release in many classes of neurons.[23] SYT14 also has TM, C2A, and C2B domains, but it has no conserved Ca^{2+}-binding motif that includes the conserved aspartic acid residues in loops 1 and 3 of C2A and C2B.[26] Although the roles of SYTs as Ca^{2+} sensors have been studied extensively, little is known about Ca^{2+}-independent SYTs, which might inhibit the SNARE-catalyzed fusion in both the absence and presence of Ca^{2+}.[27] Recently, Zhang et al.[28] suggested that Ca^{2+}-independent SYT4 (MIM 600103) negatively regulates exocytosis, regardless of its inability to induce Ca^{2+}-dependent exocytosis.

SYT14 has phospholipid-binding activity that is Ca^{2+} independent.[14] The glycine residue mutated in the family is located around the C2B domain loop 1, which plays an important role in binding to phospholipids in SYT1.[25] We confirmed that, compared to the wild-type, the mutation did not alter the binding activity of SYT14 to phospholipids. In an overexpression system, wild-type SYT14 as well as normal variants were distributed in the cytoplasm close to the plasma membrane, showing in-line accumulation along with the membrane. In contrast, the p.Gly484Asp mutant showed a different (reticular) distribution pattern. In the ER, several cotranslational and posttranslational modifications that are required for the correct folding of transmembrane and secretory proteins take place.[29,30] Incompletely folded proteins are generally excluded from ER exit sites.[29] The fact that the p.Gly484Asp was not properly transferred from the ER suggests that the mutant protein might not fold correctly. The lower yield of the mutant protein as compared to the wild-type in the bacterial expression system we performed also supports the improper folding of the mutant. Abnormal distribution in the ER might result in the loss of function of SYT14 or in ER dysfunction.

In conclusion we have shown that SYT14 is localized specifically in Purkinje cells of mouse and human cerebellum. The results strongly support the involvement of SYT14 in the pathogenesis of SCA and are consistent with the atrophy of the cerebellum seen in both patients. A possible relationship between SYTs and neurodegeneration has been suggested previously,[31] and here we provide data that support the idea that disruption of an SYT protein is involved in human neurodegeneration and that exocytosis machinery can be involved in one of the pathomechanisms of neurodegeneration.

Supplemental Data

Supplemental Data include two figures and five tables and can be found with this article online at http://www.cell.com/AJHG/.

Acknowledgments

We would like to thank the patients and their family for their participation in this study. We are indebted to Syu-ichi Hirai (Department of Molecular Biology, Yokohama City University) for providing useful technical information about subcellular fractionation and to Keiko Yamaoka (Kanagawa Rehabilitation Center) for providing brain tissue from the control subject. This work was supported by research grants from the Ministry of Health, Labour, and Welfare (H.S., N. Miyake, and N. Matsumoto), the Japan Science and Technology Agency (N. Matsumoto), a Grant-in-Aid for Scientific Research from the Japan Society for the Promotion of Science (N. Matsumoto), a Grant-in-Aid for Young Scientist from the Japan Society for the Promotion of Science (H.D., N. Miyake, and H.S.) and a grant-in-aid from The Kimi Imai Memorial Foundation for Research of Incurable Neuromuscular Diseases (H.D.).

Received: June 4, 2011
Revised: July 11, 2011
Accepted: July 15, 2011
Published online: August 11, 2011

Web Resources

The URLs for data presented herein are as follows:

Align GVGD, http://agvgd.iarc.fr/
Allen Human brain Atlas, http://human.brain-map.org/
Allen Mouse Brain Atlas, http://mouse.brain-map.org/
HomozygosityMapper, http://www.homozygositymapper.org/
Online Mendelian Inheritance in Man (OMIM), http://www.omim.org/
PolyPhen, http://genetics.bwh.harvard.edu/pph/
PolyPhen2, http://genetics.bwh.harvard.edu/pph2/
SIFT, http://blocks.fhcrc.org/sift/SIFT.html

Rerefences

1. Fogel, B.L., and Perlman, S. (2007). Clinical features and molecular genetics of autosomal recessive cerebellar ataxias. Lancet Neurol. *6*, 245–257.
2. Palau, F., and Espinós, C. (2006). Autosomal recessive cerebellar ataxias. Orphanet J. Rare Dis. *1*, 47.
3. Embiruçu, E.K., Martyn, M.L., Schlesinger, D., and Kok, F. (2009). Autosomal recessive ataxias: 20 types, and counting. Arq. Neuropsiquiatr. *67*, 1143–1156.
4. Anheim, M., Fleury, M., Monga, B., Laugel, V., Chaigne, D., Rodier, G., Ginglinger, E., Boulay, C., Courtois, S., Drouot, N., et al. (2010). Epidemiological, clinical, paraclinical and

molecular study of a cohort of 102 patients affected with autosomal recessive progressive cerebellar ataxia from Alsace, Eastern France: Implications for clinical management. Neurogenetics *11*, 1–12.
5. Manto, M., and Marmolino, D. (2009). Cerebellar ataxias. Curr. Opin. Neurol. *22*, 419–429.
6. Vermeer, S., Hoischen, A., Meijer, R.P., Gilissen, C., Neveling, K., Wieskamp, N., de Brouwer, A., Koenig, M., Anheim, M., Assoum, M., et al. (2010). Targeted next-generation sequencing of a 12.5 Mb homozygous region reveals *ANO10* mutations in patients with autosomal-recessive cerebellar ataxia. Am. J. Hum. Genet. *87*, 813–819.
7. Seelow, D., Schuelke, M., Hildebrandt, F., and Nurnberg, P. (2009). HomozygosityMapper—An interactive approach to homozygosity mapping. Nucleic Acids Res. *37*, W593–W599.
8. Bahlo, M., and Bromhead, C.J. (2009). Generating linkage mapping files from Affymetrix SNP chip data. Bioinformatics *25*, 1961–1962.
9. Gudbjartsson, D.F., Thorvaldsson, T., Kong, A., Gunnarsson, G., and Ingolfsdottir, A. (2005). Allegro version 2. Nat. Genet. *37*, 1015–1016.
10. Li, H., Ruan, J., and Durbin, R. (2008). Mapping short DNA sequencing reads and calling variants using mapping quality scores. Genome Res. *18*, 1851–1858.
11. Gilissen, C., Arts, H.H., Hoischen, A., Spruijt, L., Mans, D.A., Arts, P., van Lier, B., Steehouwer, M., van Reeuwijk, J., Kant, S.G., et al. (2010). Exome sequencing identifies *WDR35* variants involved in Sensenbrenner syndrome. Am. J. Hum. Genet. *87*, 418–423.
12. Tsurusaki, Y., Osaka, H., Hamanoue, H., Shimbo, H., Tsuji, M., Doi, H., Saitsu, H., Matsumoto, N., and Miyake, N. (2011). Rapid detection of a mutation causing X-linked leucoencephalopathy by exome sequencing. J. Med. Genet., in press. Published online March 17, 2011. 10.1136/jmg.2010.083535.
13. Becker, J., Semler, O., Gilissen, C., Li, Y., Bolz, H.J., Giunta, C., Bergmann, C., Rohrbach, M., Koerber, F., Zimmermann, K., et al. (2011). Exome sequencing identifies truncating mutations in human *SERPINF1* in autosomal-recessive osteogenesis imperfecta. Am. J. Hum. Genet. *88*, 362–371.
14. Fukuda, M. (2003). Molecular cloning, expression, and characterization of a novel class of synaptotagmin (Syt XIV) conserved from *Drosophila* to humans. J. Biochem. *133*, 641–649.
15. Adolfsen, B., Saraswati, S., Yoshihara, M., and Littleton, J.T. (2004). Synaptotagmins are trafficked to distinct subcellular domains including the postsynaptic compartment. J. Cell Biol. *166*, 249–260.
16. Quintero-Rivera, F., Chan, A., Donovan, D.J., Gusella, J.F., and Ligon, A.H. (2007). Disruption of a synaptotagmin (*SYT14*) associated with neurodevelopmental abnormalities. Am. J. Med. Genet. A. *143*, 558–563.
17. Michelsen, U., and von Hagen, J. (2009). Isolation of subcellular organelles and structures. Methods Enzymol. *463*, 305–328.
18. Fukuda, M., Kojima, T., and Mikoshiba, K. (1996). Phospholipid composition dependence of Ca^{2+}-dependent phospholipid binding to the C2A domain of synaptotagmin IV. J. Biol. Chem. *271*, 8430–8434.
19. Doi, H., Mitsui, K., Kurosawa, M., Machida, Y., Kuroiwa, Y., and Nukina, N. (2004). Identification of ubiquitin-interacting proteins in purified polyglutamine aggregates. FEBS Lett. *571*, 171–176.
20. Jana, N.R., Tanaka, M., Wang, G., and Nukina, N. (2000). Polyglutamine length-dependent interaction of Hsp40 and Hsp70 family chaperones with truncated N-terminal huntingtin: Their role in suppression of aggregation and cellular toxicity. Hum. Mol. Genet. *9*, 2009–2018.
21. Oyama, F., Miyazaki, H., Sakamoto, N., Becquet, C., Machida, Y., Kaneko, K., Uchikawa, C., Suzuki, T., Kurosawa, M., Ikeda, T., et al. (2006). Sodium channel beta4 subunit: down-regulation and possible involvement in neuritic degeneration in Huntington's disease transgenic mice. J. Neurochem. *98*, 518–529.
22. Gros-Louis, F., Dupré, N., Dion, P., Fox, M.A., Laurent, S., Verreault, S., Sanes, J.R., Bouchard, J.P., and Rouleau, G.A. (2007). Mutations in *SYNE1* lead to a newly discovered form of autosomal recessive cerebellar ataxia. Nat. Genet. *39*, 80–85.
23. McCue, H.V., Haynes, L.P., and Burgoyne, R.D. (2010). The diversity of calcium sensor proteins in the regulation of neuronal function. Cold Spring Harb. Perspect. Biol. *2*, a004085.
24. Bai, J., and Chapman, E.R. (2004). The C2 domains of synaptotagmin—partners in exocytosis. Trends Biochem. Sci. *29*, 143–151.
25. Chapman, E.R. (2008). How does synaptotagmin trigger neurotransmitter release? Annu. Rev. Biochem. *77*, 615–641.
26. Rickman, C., Craxton, M., Osborne, S., and Davletov, B. (2004). Comparative analysis of tandem C2 domains from the mammalian synaptotagmin family. Biochem. J. *378*, 681–686.
27. Bhalla, A., Chicka, M.C., and Chapman, E.R. (2008). Analysis of the synaptotagmin family during reconstituted membrane fusion. Uncovering a class of inhibitory isoforms. J. Biol. Chem. *283*, 21799–21807.
28. Zhang, G., Bai, H., Zhang, H., Dean, C., Wu, Q., Li, J., Guariglia, S., Meng, Q., and Cai, D. (2011). Neuropeptide exocytosis involving synaptotagmin-4 and oxytocin in hypothalamic programming of body weight and energy balance. Neuron *69*, 523–535.
29. Ellgaard, L., and Helenius, A. (2003). Quality control in the endoplasmic reticulum. Nat. Rev. Mol. Cell Biol. *4*, 181–191.
30. Colgan, S.M., Hashimi, A.A., and Austin, R.C. (2011). Endoplasmic reticulum stress and lipid dysregulation. Expert Rev. Mol. Med. *13*, e4.
31. Glavan, G., Schliebs, R., and Zivin, M. (2009). Synaptotagmins in neurodegeneration. Anat. Rec. (Hoboken) *292*, 1849–1862.
32. Schmitz-Hübsch, T., du Montcel, S.T., Baliko, L., Berciano, J., Boesch, S., Depondt, C., Giunti, P., Globas, C., Infante, J., Kang, J.S., et al. (2006). Scale for the assessment and rating of ataxia: Development of a new clinical scale. Neurology *66*, 1717–1720.

Hum Genet
DOI 10.1007/s00439-011-1105-7

ORIGINAL INVESTIGATION

Rapid detection of gene mutations responsible for non-syndromic aortic aneurysm and dissection using two different methods: resequencing microarray technology and next-generation sequencing

Haruya Sakai · Shinichi Suzuki · Takeshi Mizuguchi · Kiyotaka Imoto · Yuki Yamashita · Hiroshi Doi · Masakazu Kikuchi · Yoshinori Tsurusaki · Hirotomo Saitsu · Noriko Miyake · Munetaka Masuda · Naomichi Matsumoto

Received: 14 July 2011 / Accepted: 4 October 2011

Abstract Aortic aneurysm and/or dissection (AAD) is a life-threatening condition, and several syndromes are known to be related to AAD. In this study, two new technologies, resequencing array technology (ResAT) and next-generation sequencing (NGS), were used to analyze eight genes associated with syndromic AAD in 70 patients with non-syndromic AAD. Eighteen sequence variants were detected using both ResAT and NGS. In addition one of these sequence variants was detected by ResAT only and two additional variants by NGS only. Three of the 18 variants are likely to be pathogenic (in 4.3% of AAD patients and in 8.6% of a subset of patients with thoracic AAD), highlighting the importance of genetic analysis in non-syndromic AAD. ResAT and NGS similarly detected most, but not all, of the variants. Resequencing array technology was a rapid and efficient method for detecting most nucleotide substitutions, but was unable to detect short insertions/deletions, and it is impractical to update custom arrays frequently. Next-generation sequencing was able to detect almost all types of mutation, but requires improved informatics methods.

Electronic supplementary material The online version of this article (doi:10.1007/s00439-011-1105-7) contains supplementary material, which is available to authorized users.

H. Sakai · T. Mizuguchi · Y. Yamashita · H. Doi · M. Kikuchi · Y. Tsurusaki · H. Saitsu · N. Miyake · N. Matsumoto (✉)
Department of Human Genetics, Yokohama City University Graduate School of Medicine, 3-9 Fukuura, Kanazawa-ku, Yokohama 236-0004, Japan
e-mail: naomat@yokohama-cu.ac.jp

S. Suzuki · M. Masuda
Department of Surgery, Yokohama City University Graduate School of Medicine, Yokohama, Japan

K. Imoto
Cardiovascular Center, Yokohama City University Medical Center, 4-57 Urafune, Minami-ku, Yokohama 232-0024, Japan

Introduction

Aortic aneurysm and/or dissection (AAD) is a life-threatening condition. As significant symptoms do not usually appear before the rupture of the AAD, which can be lethal, it is often difficult to prevent death from AAD. Timely cardiovascular surgery may prevent AAD rupture and save the patient's life. Approximately 20% of patients with thoracic aortic disease have a family history of the disease, which is typically inherited in an autosomal dominant manner with decreased penetrance and variable expressivity (Wang et al. 2010). Therefore, if a causative mutation is detected in a patient, it is worth checking for the mutation in their asymptomatic family members to prevent future aortic events by medical and/or surgical intervention. Several genes are known to be associated with syndromes presenting with hereditary AAD and vascular disruption: *FBN1* (Dietz et al. 1991; Lee et al. 1991a), *TGFBR2* (Mizuguchi et al. 2004), *TGFBR1* (Loeys et al. 2005), *MYH11* (Zhu et al. 2006), *ACTA2* (Guo et al. 2007), *COL3A1* (Superti-Furga et al. 1988), *PLOD1* (Hautala et al. 1993), and *SLC2A10* (Coucke et al. 2006) (Table 1). Most AAD patients who have been surgically treated are not affected by these syndromes. However, the contribution of these genes to non-syndromic AAD has not been thoroughly investigated. A comprehensive study of these genes by conventional Sanger sequencing is a huge and expensive undertaking. Even high-resolution melting methods and denaturing high performance liquid chromatography require the amplification of at least 210 exons from these eight genes (Table 1). Therefore, it has been unrealistic for most laboratories to analyze these genes in multiple samples.

Published online: 15 October 2011

Table 1 Overview of genes associated with AAD analyzed in this study

Gene	GenBank accession no.	Disorder	Type	Exon (CDE)	ORF (bp)	Amplicon
FBN1	NM_000138	MFS, SGS, TAAD	AD	66 (65)	8,616	39
TGFBR2	NM_001024847	MFS2, LDS, SGS, TAAD	AD	8 (8)	1,779	8
TGFBR1	NM_004612	MFS2, LDS, SGS, TAAD	AD	9 (9)	1,512	7
COL3A1	NM_000090	EDS type IV	AD	51 (51)	4,401	16
PLOD1	NM_000302	EDS type VI	AR	19 (19)	2,184	13
MYH11	NM_001040113	TAAD	AD	43 (41)	5,838	30
SLC2A10	NM_030777	ATS	AR	5 (5)	1,626	5
ACTA2	NM_001613	TAAD	AD	9 (8)	1,134	6

CDE coding exon, *ORF* open reading frame, *MFS* Marfan syndrome, *MFS2* Marfan syndrome type II, *LDS* Loeys–Dietz syndrome, *SGS* Shprintzen–Goldberg syndrome, *TAAD* thoracic aortic aneurysm and dissection, *EDS* Ehlers–Danlos syndrome, *ATS* arterial tortuosity syndrome, *AD* autosomal dominant, *AR* autosomal recessive

Resequencing array technology (ResAT) enables the investigation of multiple genes on one chip. This technology has been used for multiple-gene analysis in childhood hearing loss (Kothiyal et al. 2010), breast-ovarian cancer syndrome (Schroeder et al. 2010), dilated cardiomyopathy (Zimmerman et al. 2010), X-linked intellectual disability (Jensen et al. 2011), familial hypercholesterolemia (Chiou et al. 2011), and hypertrophic cardiomyopathy (Fokstuen et al. 2011). Different research groups have shown ResAT to be a highly efficient, relatively accurate, cost-effective, and rapid method. However, several drawbacks have been pointed out, including its insensitivity in detecting nucleotide insertions/deletions (indels) and nucleotide changes in GC-rich regions and repeat sequences.

Next-generation sequencing (NGS) is now regarded as the most powerful technology for detecting mutations (Ng et al. 2010; Tsurusaki et al. 2011). This platform is advantageous in finding almost all types of mutations including small indel mutations. The high throughput and multiplexing of NGS allows multiple genes to be sequenced in many samples in a single run (Farias-Hesson et al. 2010; Gabriel et al. 2009).

In this study, we analyzed the eight AAD-associated genes (*FBN1*, *TGFBR2*, *TGFBR1*, *COL3A1*, *PLOD1*, *MYH11*, *SLC2A10*, and *ACTA2*) in 70 patients with non-syndromic AAD by two methods: ResAT (all eight genes on one chip) and multiplex NGS. We describe here a comparison of the results.

Materials and methods

Patients

Seventy Japanese patients, who had surgery for AAD, were recruited from Yokohama City University Hospital and Yokohama City University Medical Center. The patients' clinical information is summarized in Table 2. Thoracic AAD involves the aorta above the diaphragm and abdominal AAD is located along the portion of the aorta passing through the abdomen. None of the patients in this study had any clinical test results supporting a diagnosis of syndromic AAD. Experimental protocols were approved by the Institutional Review Board of Yokohama City University School of Medicine. Informed consent for genetic analysis was obtained from the patients. DNA was extracted from peripheral blood leukocytes using a QuickGene-610L kit (Fujifilm, Tokyo, Japan).

Table 2 Clinical information of AAD patients

Clinical data	Number of patients (%)
Thoracic AAD[a]	35 (50.0)
Abdominal AAD[a]	30 (42.9)
Thoracic and abdominal AAD[a]	5 (7.1)
Age (years) (mean ± SD)	67.3 ± 10.2 (range 39–83)
Age (years) (median)	68.5
<50 years old	4 (5.7)
50–54 years old	5 (7.1)
55–59 years old	8 (11.4)
≥60 years old	53 (75.7)
Male	53 (75.7)
Female	17 (24.3)
Diabetes	9 (12.9)
Hyperlipidemia	32 (45.7)
Hypertension	54 (77.1)
Current smoker	15 (21.4)
Past smoker	30 (42.9)
Never smoked	23 (32.9)

[a] Including current and past operations

Array design

Eight genes (*FBN1*, *TGFBR2*, *TGFBR1*, *COL3A1*, *PLOD1*, *MYH11*, *SLC2A10* and *ACTA2*) (Table 1) associated with AAD were selected for one custom chip (Affymetrix, Santa Clara, CA). All coding exons as well as 29 bp of sequence from each intron (21 bp on the 5′-side and 8 bp on the 3′-side of each exon) were analyzed. Repetitive sequences and intragenic low complexity regions larger than 25 bp were excluded from the chip. A total of 33,116 bp from the eight genes could be sequenced using this chip.

PCR amplification, purification, hybridization, scanning, and data analysis

The targeted regions were amplified as 124 fragments by PCR (ranging from 965 to 2,999 bp) using Blend Taq Plus (TOYOBO, Osaka, Japan) or KOD FX (TOYOBO) and genomic DNA as a template in a 20 μL volume. The PCR conditions were: denaturing at 94°C, 35 cycles of 94°C for 30 s, 62°C for 30 s, and 72°C for 3 min, and a final extension at 72°C for 7 min. The DNA concentration of the amplicons was determined using a Quant-iT PicoGreen dsDNA Assay Kit (Invitrogen, Carlsbad, CA, USA) with a Spectra Fluor F129003 (Tecan, Männedorf, Switzerland). The PCR amplicons were pooled in equimolar quantities (110 fmol). The mixed samples were purified and the volume was reduced using a Microcon YM-100 filter (Millipore, Brussels, Belgium). Fragmentation of the products, labeling with biotin, hybridization, washing, and scanning procedures were carried out based on the CustomSeq resequencing array protocol version 2.1 (Affymetrix). An FS450 fluidics station (Affymetrix) was used for washing and staining and a GCS3000 7G scanner (Affymetrix) was used for scanning. To test the efficiency of mutation detection, PCR products containing 20 known heterozygous mutations (Table 3) from three genes (*FBN1, TGFBR2*, and *TGFBR1*), as well as another 104 PCR products amplified from normal control DNA, covering all the other exons, were analyzed using the chip. Affymetrix GCOS and GSEQ software were used to process the raw data and analyze the nucleotide sequences, respectively. The default settings of GSEQ were adopted.

Multiplex next-generation sequencing

The PCR amplicons from one patient were mixed and processed using a multiplexing sequencing primers and PhiX control kit (Illumina, San Diego, CA, USA) according to the manufacturer's instructions but with minor changes. In brief, amplicons were fragmented with Covaris S1 (Covaris, Woburn, MA, USA), and purified using Agencourt AMPure (Beckman Coulter, Brea, CA, USA) instead of gel extraction. DNA quality was checked with an Agilent 2100 bioanalyzer (Agilent Technologies, Santa Clara, CA, USA) and a bar code DNA tag (Illumina) was ligated on. The bar code DNA tags contain unique 6 bp sequences and allow the processing of up to 96 DNA fragments in a single run using an Illumina GAIIx (Illumina). Twelve processed DNA fragments, each with a different tag, were mixed and analyzed with single 76 bp reads in one lane of the flow cell. Six lanes were necessary for the analysis of 70 samples. Image analysis and base calling were performed by sequence control software real-time analysis (Illumina) and offline Basecaller software v1.8.0 (Illumina). The reads were aligned to the human reference genome sequence (UCSC hg19, GRCh37) using the ELAND v2 algorithm in CASAVA software v1.7.0 (Illumina).

Table 3 Known mutations used as positive controls for testing ResAT

Nucleotide substitution		Small deletion or insertion	
Gene	Mutation	Gene	Mutation
FBN1	c.400T > G	*FBN1*	c.937delT
	c.772C > T		c.1876delG
	c.1011C > A		c.4283–4284insG
	c.1285C > T		c.7039–7040delAT
	c.2413T > C		
	c.2942G > C		
	c.4099T > C		
	c.4495A > T		
	c.5539T > C		
	c.5788G + 5G > A		
	c.6236C > G		
	c.6773G > A		
TGFBR2	c.1142G > C		
	c.1411G > A		
	c.1624C > T		
TGFBR1	c.1135A > G		

All mutations are previously reported (Sakai et al. 2006; Togashi et al. 2007)

Mapping strategy and variant annotation

An average of 2.4 million reads (ranging from 1.7 to 4.0 million reads) for each sample passed quality control (Path Filter) and were mapped to the human reference genome using mapping and assembly with qualities (MAQ) (Li et al. 2008), NextGENe software v2.00 (SoftGenetics, State College, PA, USA), and Burrows-Wheeler Aligner (BWA)/sequence alignment/map tools (SAMtools) (Li and Durbin 2010; Li et al. 2009). Single nucleotide polymorphisms (SNPs) and indels were extracted from the alignment data using an original script created by BITS, Tokyo, Japan along with information on the registered SNPs (dbSNP131). A consensus quality score of 40 or more was used for the

SNP analysis in MAQ. SNPs in MAQ-passed reads were annotated using the SeattleSeq website (http://gvs.gs.washington.edu/SeattleSeqAnnotation/). A minimum base quality of 13, a minimum root mean square mapping quality for SNPs of 10, and a minimum read depth of 2 were used in BWA/SAMtools (Li and Durbin 2010; Li et al. 2009). NextGENe (SoftGenetics) was also used to analyze the reads, employing default settings apart from using the no-condensation mode. For base substitutions, we focused on variants detected in common by both MAQ and NextGENe. Small indel variants were classified as positive if found by both BWA and NextGENe.

Validation of novel variants

Novel variants (not in dbSNP131, the 1,000 genomes dataset or our in-house database) identified by ResAT and NGS were validated by Sanger sequencing. Surplus PCR products were treated with ExoSAP IT (GE Healthcare, Piscataway, NJ) and sequenced using a standard protocol using BigDye terminators (Applied Biosystems, Foster City, CA, USA) on an ABI PRISM 3100 genetic analyzer (Applied Biosystems). Furthermore, novel variants were screened in 94 Japanese controls by high-resolution melt curve analysis (LightCycler 480; Roche Diagnostics, Basel, Switzerland) and subsequent Sanger sequencing. Novel variants were evaluated using web-based programs including PolyPhen (http://genetics.bwh.harvard.edu/pph/), PolyPhen2 (http://genetics.bwh.harvard.edu/pph2/), Mutation Taster (http://www.mutationtaster.org/), and ESEfinder (http://rulai.cshl.edu/cgi-bin/tools/ESE3/esefinder.cgi?process=home).

Results

Array performance

Across all 70 samples, the mean nucleotide call rate was 95.7% (range 87.3–97.6%) using the default settings of GSEQ. We observed an improvement of the call rate as the number of samples increased. For example, the call rate by GCOS for the first two samples was 90.1 and 90.6% and was 93.3 and 93.9% when 10 samples were analyzed, and was 94.9 and 95.5% when 33 samples were analyzed. However, between 34 and 70 samples, the call rate did not greatly improve (only by 1%). We had constant difficulty in reading approximately 4% of the sequences per array (i.e., no sequence called), mostly in regions of high GC and CC content.

Detection of known mutations by ResAT

To validate the quality of mutation detection in our resequencing array, we analyzed amplicons containing 16 known nucleotide substitutions, three small deletions (1–2 bp), and one 1 bp insertion, plus all the other normal exons (Sakai et al. 2006; Togashi et al. 2007) (Table 3). Fourteen out of 16 nucleotide substitutions were detected (87.5%) by GSEQ in the automated mode. Two mutations (c.772C > T in *FBN1* and c.1142G > C in *TGFBR2*) were not detected. The former was insensitive, and the latter was indicated as a no-call. Visual inspection in the manual mode enabled easy detection of the *TGFBR2* mutation. The mutation detection rate was 93.8% (15/16) using both the automated and manual modes. None of the small indels were detected by our array in either the automated or manual modes.

Variant detection by ResAT

We detected 70 nucleotide substitutions in the automated mode in the 70 patients analyzed (0–3 variants per sample). Fifty-one variants were already registered in dbSNP131 and/or in our in-house database (Supplementary table). The remaining 19 novel variants were validated by Sanger sequencing (Table 4). One variant (c.976–16C > T in *PLOD1*) was homozygous and the others were heterozygous. No indel mutations were detected.

Variant detection by NGS

The target regions were completely covered by NGS reads (100%). The average read depth (coverage of sequence reads) was approximately 600 for each gene (Table 5). The NextGENe software detected a mean of 876 variants in the 70 patients with mutation scores of 10 or more (ranging from 581 to 1209 with SD = 131). MAQ and SeattelSeq detected a mean of 271 variants (ranging from 111 to 384 with SD = 52). Semi-automatic exclusion of variants that were out of the target regions (22 bp or more away from the 5′-end of exons and 9 bp or more away from the 3′-end of exons) or were known variants in dbSNP131 was performed using Excel 2008 for Mac (Microsoft, Redmond, WA, USA), narrowing the data down to 0–6 variants per sample. Twenty novel variants were detected by both MAQ and NextGENe, which were further validated by Sanger sequencing. No indel mutations were detected by MAQ, NextGENe, or BWA/SAMtools.

Comparison of ResAT and NGS variants

Eighteen novel variants were detected by ResAT and NGS. One was detected by ResAT only and two by NGS only. The two variants undetected by ResAT were c.1388G > A (p.Arg463Gln) in *PLOD1* and c.136A > C (p.Ser46Arg) in *TGFBR2*. The former was indicated as a no-call, but was detected later in the manual mode. The latter was within a

Table 4 Novel variants detected by ResAT and/or NGS

Mutation		Amino acid change	Methods of detection	Read depth in NGS	PolyPhen	PolyPhen2	Mutation taster	Patients	Controls (total number)
Gene	Mutation								
TGFBR2	*c.136A > C*[c]	p.Ser46Arg	NGS	472	Benign	Benign (0.099)	Polymorphism	1	0 (94)
	c.403G > T	p.Asp135Tyr	ResAT and NGS	1,257	Possibly damaging	Possibly damaging (0.682)	Polymorphism	1	0 (94)
	c.692C > T[d]	p.Thr231Met	ResAT and NGS	989	Benign	Possibly damaging (0.670)	Polymorphism	1	0 (93)
TGFBR1	*c.1032T > C*	p.Asn344Asn	ResAT and NGS	939	Unknown	–	Polymorphism	1	3 (94)
COL3A1	*c.1815 + 5G > A*		ResAT	255	Unknown	–	Disease-causing	1	0 (94)
	c.84T > C[d]	p.Val28Val	ResAT and NGS	644	Unknown	–	Polymorphism	1	0 (94)
	c.119C > T[c]	p.Ala40Val	ResAT and NGS	1,402	Unknown	Unknown	Polymorphism	1	0 (94)
	c.3133G > A	p.Ala1045Thr	ResAT and NGS	630	Benign	Probably damaging (0.979)	Polymorphism	1	0 (94)
	c.3776C > T	p.Ala1259Val	ResAT and NGS	872	Unknown	Unknown	Disease-causing	1	0 (94)
PLOD1	*c.976–16C > T*[a]		ResAT and NGS	631	unknown	–	polymorphism	1	2[a] (94)
	c.1098–8C > G		ResAT and NGS	633	Unknown	–	Disease-causing	1	0 (94)
	c.1388G > A	p.Arg463Gln	NGS	624, 768	Unknown	Probably damaging (0.961)	Disease-causing	2	4 (94)
	c.1495C > T	p.Arg499Trp	ResAT and NGS	509, 532, 568, 679	Probably damaging	Probably damaging (0.992)	Disease-causing	4	2 (94)
MYH11	*c.4600–13G > A*		ResAT and NGS	1,336	unknown	–	Polymorphism	1	2 (94)
	c.4625G > A[b]	p.Arg1542Gln	ResAT and NGS	1,254	Possibly damaging	Probably damaging (0.994)	Disease-causing	1	0 (94)
	c.4963C > T[b]	p.Arg1655Cys	ResAT and NGS	2,711	Probably damaging	Probably damaging (1.000)	Disease-causing	1	0 (94)
SLC2A10	*c.315C > T*	p.Arg105Arg	ResAT and NGS	543	Unknown	–	Polymorphism	1	0 (94)
	c.330C > T[e]	p.Phe110Phe	ResAT and NGS	500	Unknown	–	Polymorphism	1	0 (94)
	c.1220T > G[b]	p.Leu407Arg	ResAT and NGS	382	Benign	possibly damaging (0.925)	Disease-causing	1	0 (94)
ACTA2	*c.130–18T > C*[c]		ResAT and NGS	607, 647	Unknown	–	Polymorphism	2	2 (94)
	c.482T > C	p.Val161Ala	ResAT and NGS	752	Probably damaging	Beningn (0.013)	Disease-causing	1	0 (94)

The underlined mutation is highly likely to be pathogenic

[a] Homozygous substitution

[b] Mutations detected in patient 16 patient

[c] Mutations detected in patient 24

[d] Mutations detected in patient 28

[e] Mutations detected in patient 89

Table 5 Gene-based read depth in NGS

Gene	Mean depth[a]
FBN1	655
TGFBR2	613
TGFBR1	568
COL3A1	596
PLOD1	607
MYH11	643
SLC2A10	571
ACTA2	543

[a] Based on NextGENe calculation

repetitive sequence. One variant (c.1815 + 5G > A in *COL3A1*) was undetected by NGS due to our set criteria (the variant was detected by MAQ, but not by NextGENe or BWA/SAMtools).

Pathological significance of the variants

We realized that none of the known pathogenic mutations were identified. The pathological impact of the variants was considered if none of the healthy controls showed the same change, if the variants altered evolutionarily conserved amino acids in functional repeats/domains, or if they were predicted to cause abnormal splicing resulting in protein truncation or degradation. Moreover, homozygous and compound heterozygous changes that were found in *PLOD1* and *SLC2A10* may confer autosomal recessive effects. At least three heterozygous variants were considered as putative pathogenic gene alterations (Table 6):

1. c.1815 + 5G > A in *COL3A1* (patient 29). A similar mutation, c.1815 + 5G > T, associated with the skipping of exon 25, was reported in a patient with Ehlers–Danlos syndrome type IV (EDS IV) (Lee et al. 1991b). ESEfinder suggested that the binding position of the splice donor matrix was changed similarly by c.1815 + 5G > A and c.1815 + 5G > T. Thus, C.1815 + 5G > A is highly likely to be pathogenic.
2. c.4963C > T (p.Arg1655Cys) in *MYH11* (patient 16). In addition to this mutation, the patient had two novel heterozygous variants: c.4625G > A (p.Arg1542Gln) in *MYH11* and c.1220T > G (p.Leu407Arg) in *SLC2A10*. Mutations in *SLC2A10* cause autosomal recessive arterial tortuosity syndrome (MIM #208050) (Coucke et al. 2006), although it is unknown whether the heterozygous variant we identified would be related to this, assuming a second-hit model of recessive disease. Both p.Arg 1542Gln and p.Arg1655Cys in *MYH11* were similarly predicted to be pathogenic by three programs (PolyPhen, PolyPhen2, and Mutation Taster). These residues are located in the coiled-coil region, and both are evolutionarily conserved amino acids (Fig. 1). Paircoil2 (http://groups.csail.mit.edu/cb/paircoil2/) was used to predict the effect of variants on the parallel coiled coil fold using pairwise residue probabilities (McDonnell et al. 2006). Paircoil2 indicated that p.Arg1655Cys altered the *p* score from 0.00096 (wild type) to 0.00579 (mutation), while p.Arg1542Gln did not alter the *p* score, 0.00016 (mutation) and 0.00018 (wild type) (Fig. 1). Thus, p.Arg1655Cys was more likely than p.Arg1542Gln to be pathogenic.
3. c.482T > C (p.Val161Ala) in *ACTA2* (patient 27). The patient was found retrospectively to suffer from familial thoracic AAD. The patient has an affected brother, but his DNA was unavailable. Valine at amino acid 161 is evolutionarily conserved and located within the actin domain. However, as we could not analyze the DNA of the affected brother, it may be more appropriate to call this variant 'of unknown significance'.

Discussion

Exon-by-exon Sanger sequencing is the gold standard for genetic analysis, but multiple-gene analysis in many patients is a huge task in terms of time and cost. In this study, we applied two emerging technologies providing rapid and efficient analysis of eight genes in 70 AAD patients. We also compared the results of the two technologies.

The overall mean call rate of our custom array by GSEQ software was 95.7%, which is comparable with previous

Table 6 Pathogenic variants found in the patients

Patient ID	Sex	Mutation	Clinical diagnosis	Age[a]	Age[b]	Family history
Patient 16	M	*MYH11* c.4963C > T p.Arp1655Cys	Thoracic and abdominal AAD	80	80	None
Patient 27	F	*ACTA2* c.482T > C p.Val161Ala	Thoracic AAD	57	46	Affected brother
Patient 29	F	*COL3A1* c.1815 + 5G > A	Thoracic AAD	80	67	None

M male, *F* female

[a] At blood collection

[b] At the first surgery

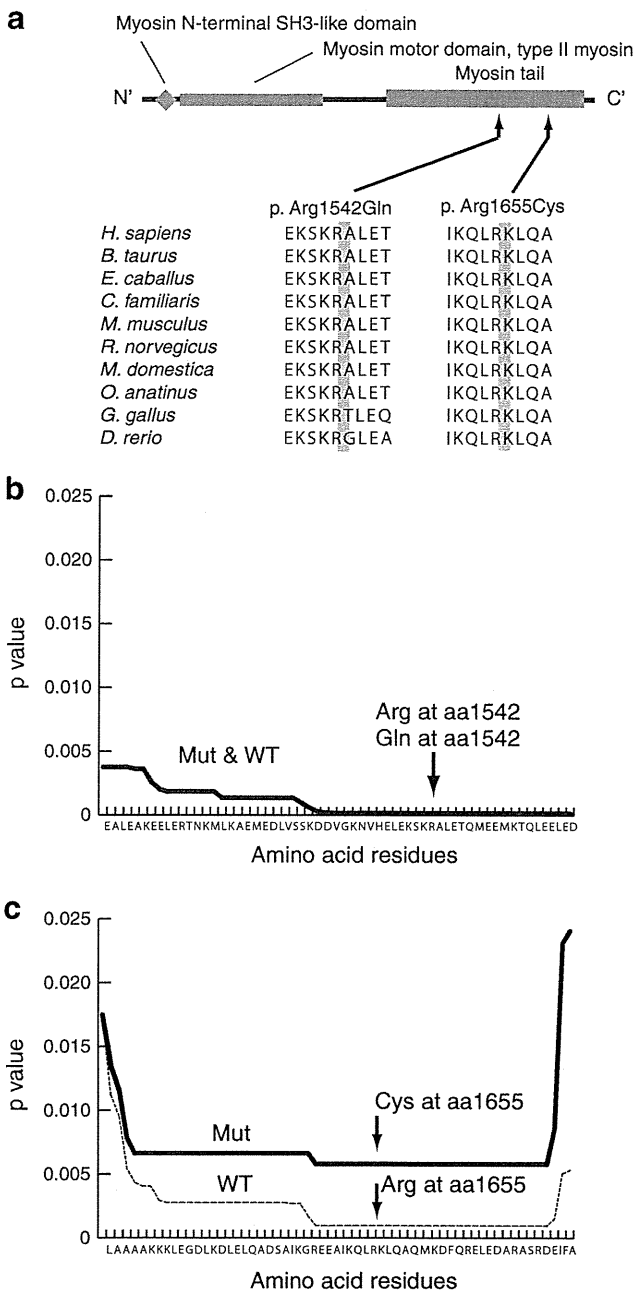

Fig. 1 Double mutations in *MYH11*. **a** Schematic representation of the MYH11 protein. Three functional domains are indicated: the myosin N-terminal SH3-like domain, the myosin motor domain for type II myosin, and the myosin tail. Both the mutations are located in the myosin tail. **b**, **c** Paircoil2 analysis showing a significantly decreased probability of coiled-coil formation for p.Arg1655Cys relative to the wild-type sequence, but no change for p.Arg1542Gln

studies (Bruce et al. 2010; Chiou et al. 2011; Jensen et al. 2011; Schroeder et al. 2010). The call rates became higher as the number of patients increased. Approximately 33 samples were necessary to attain the maximum call-rate in GSEQ. A similar observation was described previously (Fokstuen et al. 2011). No-call regions are one of the problems of ResAT. Other groups have previously suggested that most of the no-call regions are GC- and CC-rich (Bruce et al. 2010; Chiou et al. 2011; Fokstuen et al. 2011). In our custom array, approximately 4% of the target sequences were difficult to obtain (no-calls) in most of the samples.

The mean detection rate of known variants using our custom array and GSEQ with the default settings (automated analysis) was 87.5%. This rate increased to 93.8% after manual inspection. For our ResAT data, the detection rate of nucleotide substitutions in the automated mode was higher, and that in the manual mode was slightly lower, compared with detection rates in previous studies (82.1 vs. 81%, respectively, in automated mode, and 97.4 vs. 100%, respectively, in manual mode) (Bruce et al. 2010; Chiou et al. 2011). Our ResAT analysis was unable to detect any small indel mutations; this is similar to other studies (Hartmann et al. 2009; Kothiyal et al. 2010). In the human gene mutation database (HGMD; http://www.hgmd.cf.ac.uk/ac/index.php), insertions/deletions account for a substantial proportion of the total registered mutations in our genes of interest: *FBN1* 23.6%, *TGFBR2* 6.4%, *TGFBR1* 10%, *COL3A1* 12.8%, *PLOD1* 46.2%, *MYH11* 20%, *SLC2A10* 21.1%, and *ACTA* 20%. Thus, the incapability of ResAT to detect indel mutations is one of its most significant drawbacks.

Our NGS analysis missed one of 21 variants (c.1815 + 5G > A in *COL3A1*). Our protocol focused on variants identified by two different informatics methods, to increase the true-positive rate. For example, MAQ (single-end reads) can detect nucleotide substitutions well, but is not good at detecting small indels (Li et al. 2008). BWA is more sensitive at detecting small indels because it can align gapped sequence (Krawitz et al. 2010). NextGENe is based on the Burrows-Wheeler transform algorithm, which is good at detecting small indels. NGS needs more efficient informatics methods to extract all the nucleotide changes correctly with lower error rates.

In this study, concomitant variants in two genes were detected in four patients (Table 4): c.4625G > A and c.4963C > T in *MYH11*, and c.1220T > G in *SLC2A10* (patient 16); c.136A > C in *TGFBR2* and c.130–18T > C in *ACTA2* (patient 24); c.84T > C in *COL3A1* and c.692C > T in *TGFBR2* (patient 28); c.119C > T in *COL3A1* and c.330C > T in *SLC2A10* (patient 89) (Table 4). It may be quite difficult to detect variants in two or more genes by conventional methods. ResAT and NGS permitted us to find multiple variants in multiple genes easily and rapidly. Double or triple mutations in unusual clinical cases will also be found using such technologies.

Three different putative pathological mutations in a heterozygous state in three of 70 patients were found in this study (4.3%). Interestingly, all the three patients suffered from thoracic AAD. Considering only those patients with

thoracic AAD ($n = 35$), the rate increased to 8.6%. Thus, non-syndromic AAD (especially thoracic AAD) can be explained to some extent by aberrations of genes related to Mendelian disorders, although our sample size was small. Interestingly, among these three patients, only patient 29 showed hyperlipidemia and the other two (patients 16 and 27) did not, which supports the genetic origin of thoracic AAD.

In this study, we compared ResAT and NGS. Considering the drawbacks of ResAT, including its inability to detect small indels and its no-call regions, we believe that NGS is the better technology for comprehensive analysis of multiple genes, especially with improved informatics methods, as it can detect all types of mutations with no bias. Another advantage of NGS is its flexibility. Resequencing array technology requires a custom-made sequencing array. It is not easy or practical to update arrays frequently. However, NGS is currently quite expensive for most laboratories. Next-generation sequencing combined with the pooled genomic DNA method with indexing may improve its cost-effectiveness (Calvo et al. 2010; Druley et al. 2009).

In conclusion, we found that 4.3% of non-syndromic AAD patients (8.5% of thoracic AAD patients) have abnormalities in genes that cause Mendelian disorders. ResAT and NGS enabled multiple genes to be analyzed efficiently. In addition to the 70 AAD patients, a patient with familial Marfan syndrome and a patient with Loeys–Dietz syndrome were initially included before their diagnosis was known. We detected c.6793T > G (p.Cys2265Gly) in *FBN1* in the Marfan syndrome patient [by ResAT (NGS was not done)] and c.797A > G (p.Asp266Gly) in *TGFBR1* in the Loeys–Dietz patient (by ResAT and NGS). We excluded these two patients from this study because they are syndromic AAD patients, but the efficient detection of their mutations highlights the validity of our approach. Finally, high throughput technologies have the potential to routinely identify novel variants of known or unknown significance in clinical settings. Therefore, more sophisticated methods to evaluate gene variants as well as databases containing normal (rare) variants are needed.

Acknowledgments The authors would like to thank the patients for their participation in this study. This work was supported by research grants from the Ministry of Health, Labour and Welfare (N. Matsumoto), the Japanese Science and Technology Agency (N. Matsumoto), the Takeda Science Foundation (N. Matsumoto), the Japanese Prize Foundation (T. Mizuguchi) and a Grant-in-Aid for Scientific Research from the Japanese Society for the Promotion of Science (N. Matsumoto).

References

Bruce CK, Smith M, Rahman F, Liu ZF, McMullan DJ, Ball S, Hartley J, Kroos MA, Heptinstall L, Reuser AJ, Rolfs A, Hendriksz C, Kelly DA, Barrett TG, MacDonald F, Maher ER, Gissen P (2010) Design and validation of a metabolic disorder resequencing microarray (BRUM1). Hum Mutat 31:858–865

Calvo SE, Tucker EJ, Compton AG, Kirby DM, Crawford G, Burtt NP, Rivas M, Guiducci C, Bruno DL, Goldberger OA, Redman MC, Wiltshire E, Wilson CJ, Altshuler D, Gabriel SB, Daly MJ, Thorburn DR, Mootha VK (2010) High-throughput, pooled sequencing identifies mutations in NUBPL and FOXRED1 in human complex I deficiency. Nat Genet 42:851–858

Chiou KR, Charng MJ, Chang HM (2011) Array-based resequencing for mutations causing familial hypercholesterolemia. Atherosclerosis 216(2):383–389

Coucke PJ, Willaert A, Wessels MW, Callewaert B, Zoppi N, De Backer J, Fox JE, Mancini GM, Kambouris M, Gardella R, Facchetti F, Willems PJ, Forsyth R, Dietz HC, Barlati S, Colombi M, Loeys B, De Paepe A (2006) Mutations in the facilitative glucose transporter GLUT10 alter angiogenesis and cause arterial tortuosity syndrome. Nat Genet 38:452–457

Dietz HC, Cutting GR, Pyeritz RE, Maslen CL, Sakai LY, Corson GM, Puffenberger EG, Hamosh A, Nanthakumar EJ, Curristin SM et al (1991) Marfan syndrome caused by a recurrent de novo missense mutation in the fibrillin gene. Nature 352:337–339

Druley TE, Vallania FL, Wegner DJ, Varley KE, Knowles OL, Bonds JA, Robison SW, Doniger SW, Hamvas A, Cole FS, Fay JC, Mitra RD (2009) Quantification of rare allelic variants from pooled genomic DNA. Nat Methods 6:263–265

Farias-Hesson E, Erikson J, Atkins A, Shen P, Davis RW, Scharfe C, Pourmand N (2010) Semi-automated library preparation for high-throughput DNA sequencing platforms. J Biomed Biotechnol 2010:617469

Fokstuen S, Munoz A, Melacini P, Iliceto S, Perrot A, Ozcelik C, Jeanrenaud X, Rieubland C, Farr M, Faber L, Sigwart U, Mach F, Lerch R, Antonarakis SE, Blouin JL (2011) Rapid detection of genetic variants in hypertrophic cardiomyopathy by custom DNA resequencing array in clinical practice. J Med Genet 48(8):572–576

Gabriel C, Danzer M, Hackl C, Kopal G, Hufnagl P, Hofer K, Polin H, Stabentheiner S, Proll J (2009) Rapid high-throughput human leukocyte antigen typing by massively parallel pyrosequencing for high-resolution allele identification. Hum Immunol 70:960–964

Guo DC, Pannu H, Tran-Fadulu V, Papke CL, Yu RK, Avidan N, Bourgeois S, Estrera AL, Safi HJ, Sparks E, Amor D, Ades L, McConnell V, Willoughby CE, Abuelo D, Willing M, Lewis RA, Kim DH, Scherer S, Tung PP, Ahn C, Buja LM, Raman CS, Shete SS, Milewicz DM (2007) Mutations in smooth muscle alpha-actin (ACTA2) lead to thoracic aortic aneurysms and dissections. Nat Genet 39:1488–1493

Hartmann A, Thieme M, Nanduri LK, Stempfl T, Moehle C, Kivisild T, Oefner PJ (2009) Validation of microarray-based resequencing of 93 worldwide mitochondrial genomes. Hum Mutat 30:115–122

Hautala T, Heikkinen J, Kivirikko KI, Myllyla R (1993) A large duplication in the gene for lysyl hydroxylase accounts for the type VI variant of Ehlers–Danlos syndrome in two siblings. Genomics 15:399–404

Jensen LR, Chen W, Moser B, Lipkowitz B, Schroeder C, Musante L, Tzschach A, Kalscheuer VM, Meloni I, Raynaud M, van Esch H, Chelly J, de Brouwer AP, Hackett A, van der Haar S, Henn W, Gecz J, Riess O, Bonin M, Reinhardt R, Ropers HH, Kuss AW (2011) Hybridisation-based resequencing of 17 X-linked intellectual disability genes in 135 patients reveals novel mutations in ATRX, SLC6A8 and PQBP1. Eur J Hum Genet 19(6):717–720

Kothiyal P, Cox S, Ebert J, Husami A, Kenna MA, Greinwald JH, Aronow BJ, Rehm HL (2010) High-throughput detection of mutations responsible for childhood hearing loss using resequencing microarrays. BMC Biotechnol 10:10

Krawitz P, Rodelsperger C, Jager M, Jostins L, Bauer S, Robinson PN (2010) Microindel detection in short-read sequence data. Bioinformatics 26:722–729

Lee B, Godfrey M, Vitale E, Hori H, Mattei MG, Sarfarazi M, Tsipouras P, Ramirez F, Hollister DW (1991a) Linkage of Marfan syndrome and a phenotypically related disorder to two different fibrillin genes. Nature 352:330–334

Lee B, Vitale E, Superti-Furga A, Steinmann B, Ramirez F (1991b) G to T transversion at position +5 of a splice donor site causes skipping of the preceding exon in the type III procollagen transcripts of a patient with Ehlers-Danlos syndrome type IV. J Biol Chem 266:5256–5259

Li H, Durbin R (2010) Fast and accurate long-read alignment with Burrows-Wheeler transform. Bioinformatics 26:589–595

Li H, Ruan J, Durbin R (2008) Mapping short DNA sequencing reads and calling variants using mapping quality scores. Genome Res 18:1851–1858

Li H, Handsaker B, Wysoker A, Fennell T, Ruan J, Homer N, Marth G, Abecasis G, Durbin R (2009) The Sequence Alignment/Map format and SAMtools. Bioinformatics 25:2078–2079

Loeys BL, Chen J, Neptune ER, Judge DP, Podowski M, Holm T, Meyers J, Leitch CC, Katsanis N, Sharifi N, Xu FL, Myers LA, Spevak PJ, Cameron DE, De Backer J, Hellemans J, Chen Y, Davis EC, Webb CL, Kress W, Coucke P, Rifkin DB, De Paepe AM, Dietz HC (2005) A syndrome of altered cardiovascular, craniofacial, neurocognitive and skeletal development caused by mutations in TGFBR1 or TGFBR2. Nat Genet 37:275–281

McDonnell AV, Jiang T, Keating AE, Berger B (2006) Paircoil2: improved prediction of coiled coils from sequence. Bioinformatics 22:356–358

Mizuguchi T, Collod-Beroud G, Akiyama T, Abifadel M, Harada N, Morisaki T, Allard D, Varret M, Claustres M, Morisaki H, Ihara M, Kinoshita A, Yoshiura K, Junien C, Kajii T, Jondeau G, Ohta T, Kishino T, Furukawa Y, Nakamura Y, Niikawa N, Boileau C, Matsumoto N (2004) Heterozygous TGFBR2 mutations in Marfan syndrome. Nat Genet 36:855–860

Ng SB, Bigham AW, Buckingham KJ, Hannibal MC, McMillin MJ, Gildersleeve HI, Beck AE, Tabor HK, Cooper GM, Mefford HC, Lee C, Turner EH, Smith JD, Rieder MJ, Yoshiura K, Matsumoto N, Ohta T, Niikawa N, Nickerson DA, Bamshad MJ, Shendure J (2010) Exome sequencing identifies MLL2 mutations as a cause of Kabuki syndrome. Nat Genet 42:790–793

Sakai H, Visser R, Ikegawa S, Ito E, Numabe H, Watanabe Y, Mikami H, Kondoh T, Kitoh H, Sugiyama R, Okamoto N, Ogata T, Fodde R, Mizuno S, Takamura K, Egashira M, Sasaki N, Watanabe S, Nishimaki S, Takada F, Nagai T, Okada Y, Aoka Y, Yasuda K, Iwasa M, Kogaki S, Harada N, Mizuguchi T, Matsumoto N (2006) Comprehensive genetic analysis of relevant four genes in 49 patients with Marfan syndrome or Marfan-related phenotypes. Am J Med Genet A 140:1719–1725

Schroeder C, Stutzmann F, Weber BH, Riess O, Bonin M (2010) High-throughput resequencing in the diagnosis of BRCA1/2 mutations using oligonucleotide resequencing microarrays. Breast Cancer Res Treat 122:287–297

Superti-Furga A, Gugler E, Gitzelmann R, Steinmann B (1988) Ehlers-Danlos syndrome type IV: a multi-exon deletion in one of the two COL3A1 alleles affecting structure, stability, and processing of type III procollagen. J Biol Chem 263:6226–6232

Togashi Y, Sakoda H, Nishimura A, Matsumoto N, Hiraoka H, Matsuzawa Y (2007) A Japanese family of typical Loeys-Dietz syndrome with a TGFBR2 mutation. Intern Med 46:1995–2000

Tsurusaki Y, Osaka H, Hamanoue H, Shimbo H, Tsuji M, Doi H, Saitsu H, Matsumoto N, Miyake N (2011) Rapid detection of a mutation causing X-linked leucoencephalopathy by exome sequencing. J Med Genet 48(9):606–609

Wang L, Guo DC, Cao J, Gong L, Kamm KE, Regalado E, Li L, Shete S, He WQ, Zhu MS, Offermanns S, Gilchrist D, Elefteriades J, Stull JT, Milewicz DM (2010) Mutations in myosin light chain kinase cause familial aortic dissections. Am J Hum Genet 87:701–707

Zhu L, Vranckx R, Khau Van Kien P, Lalande A, Boisset N, Mathieu F, Wegman M, Glancy L, Gasc JM, Brunotte F, Bruneval P, Wolf JE, Michel JB, Jeunemaitre X (2006) Mutations in myosin heavy chain 11 cause a syndrome associating thoracic aortic aneurysm/aortic dissection and patent ductus arteriosus. Nat Genet 38:343–349

Zimmerman RS, Cox S, Lakdawala NK, Cirino A, Mancini-DiNardo D, Clark E, Leon A, Duffy E, White E, Baxter S, Alaamery M, Farwell L, Weiss S, Seidman CE, Seidman JG, Ho CY, Rehm HL, Funke BH (2010) A novel custom resequencing array for dilated cardiomyopathy. Genet Med 12:268–278

CLINICAL GENETICS An International Journal of Genetics, Molecular and Personalized Medicine

Clin Genet 2011: 80: 293–296
Printed in Singapore. All rights reserved

CLINICAL GENETICS
doi: 10.1111/j.1399-0004.2011.01644.x

Letter to the Editor

A novel homozygous mutation of *DARS2* may cause a severe LBSL variant

To the Editor:

Leukoencephalopathy with brain stem and spinal cord involvement, and lactate elevation (LBSL, MIM #611105) is an autosomal recessive disorder with an early childhood-to-adolescence onset. In 2003, van der Knaap et al. originally described LBSL, which is characterized by slowly progressive pyramidal, cerebellar, and dorsal column dysfunction with increased white matter lactate levels in magnetic resonance (MR) spectroscopy (1). Since the first discovery that LBSL is caused by mutations of the *DARS2* gene-encoding mitochondrial aspartyl-tRNA synthetase (MtAspRS) (2), *DARS2* mutations have been found in all the patients described (2–5), but none of them showed a homozygous mutation (all are compound heterozygotes), suggesting that the activity of mutant MtAspRS homodimers may be incompatible with human life (2, 5). Here, we describe, for the first time, a consanguineous family with a homozygous *DARS2* mutation.

Materials and methods

We analyzed a consanguineous family including three affected children diagnosed with leukoencephalopathy (Fig. 1a and Table 1). The proband (II-2) developed truncal ataxic gait at 3 years old. Her affected sister (II-3) and brother (II-4) also showed truncal ataxia at 6 and 11 months, respectively. All cases were presented with horizontal nystagmus, slurring speech, ataxic gait, muscle tonus abnormality, hypo- or hyperreflexia, and tremor as well as mental retardation. II-2 at age 21 years could slowly speak one or two words. Peripheral muscles atrophy, weakness and joints contractures in extremities, loss of deep tendons reflex and disturbed deep sensation were noted. II-3 and II-4 died of pneumonia at age 8 years and respiratory failure at age 2 years, respectively. Although there were differences in MR imaging characteristics from classical LBSL, there were also striking similarities. In our patients, the involvement of the cerebral and cerebellar white matter was more diffused and severe than in classical LBSL, but the affected brain stem and spinal cord tracts were the same (Fig. 1b and Table 1).

Linkage analysis and direct sequencing of *DARS2* were performed as previously reported (6). Immunoblotting was carried out using antihuman DARS2 antibody (ab69336, Abcam, Cambridge, UK) and anti-cytochrome *c* oxidase (COX) IV antibody (ab16056, Abcam).

Results

Homozygosity mapping of this consanguineous family revealed the largest 8.5 Mb homozygous region at chromosome 1q25.1 with the maximum LOD score of 1.329. Five additional microsatellite markers showed the consistent result (Fig. 1a). Within this region, *DARS2* gene was highlighted as the primary target as it was causative for the LBSL. We found that all affected children possessed homozygous, and parents and an unaffected sib had the heterozygous intronic change at 22 base pairs upstream of exon 3 (c.228-22T>A), respectively. This change was not observed in 395 controls. We examined its mutational effect by reverse transcriptase-polymerase chain reaction (RT-PCR) using mRNA of lymphoblastoid cell lines (LCLs) derived from the proband, her father (a carrier) and a normal control. A shorter PCR fragment which lacked the entire exon 3 was confirmed by sequencing (Fig. 1c,d). Furthermore, wild-type *DARS2* mRNA and MtAspRS protein were significantly decreased in proband's LCL (Fig. 1e,f). Other genes within the 1q25.1 region have not been checked.

Discussion

We found a novel homozygous mutation of *DARS2* in a diffuse leukoencephalopathy, which may be an LBSL variant. This change resulted in the decrease of normal protein level and may have contributed to this disease. Two possibilities for the increased severity are considered: (i) a

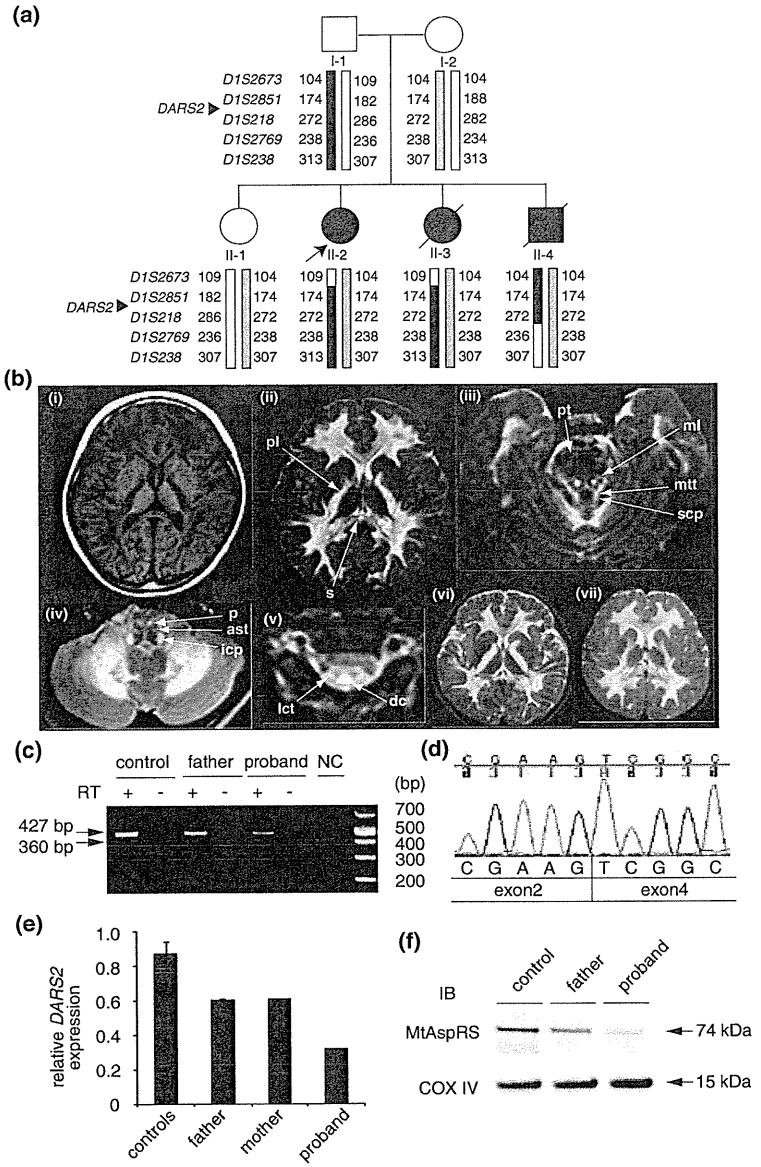

Fig. 1. Identification of a homozygous *DARS2* mutation causing abnormal splicing. (**a**) Haplotype analysis of the family. The black and gray bars represent disease alleles. The *DARS2* gene is located in between *D1S2851* and *D1S218*. (**b**) Magnetic resonance (MR) images of central nervous system in the proband (II-2) at 5 years (i–v), II-3 at 5 years (vi) and II-4 at 1 year and 4 months of age (vii). T_1-weighted (i) and T_2-weighted (T_2) (ii) images of cerebrum. The cerebral white matter was diffusely and severely affected, while the cerebral white matter involvement is less severe and more limited in extent in leukoencephalopathy with brain stem and spinal cord involvement, and lactate elevation with sparing of the U-fibers. Inhomogeneous signal abnormalities were observed in the posterior limb (pl) of the internal capsule and the splenium (s) of the corpus callosum. (iii) T_2 image at the level of the pons. The abnormal high-intensity signals were observed in pyramidal tracts (pt), medial lemniscus (ml), mesencephalic trigeminal tracts (mtt) and superior cerebellar peduncles (scp). (iv) T_2 image at the level of medulla. The pyramids (p), anterior spinocerebellar tracts (ast) and inferior cerebellar peduncles (icp) were affected. (v) T_2 image at the level of the cervical spinal cord. The dorsal columns (dc) and lateral corticospinal tracts (lct) showed abnormal signals. II-3 (vi) and II-4 (vii) showed the similar MR images as the proband. (**c**) RT-PCR using cDNA extracted from LCLs of a normal control, father and the proband. A shorter fragment (360 bp) in addition to a normal product (427 bp) was seen in father and the proband. (**d**) Electropherogram of the shorter fragment showing skipping of exon 3. (**e**) Relative expression of wild-type *DARS2* mRNA compared to β-actin mRNA in LCLs were determined by quantitative real-time RT-PCR using TaqMan Gene Expression Assays (Applied Biosystems, Bedford, MA). The relative *DARS2* expression was analyzed using TaqMan Probe (Applied Biosystems, Hs01016215_m1 for *DARS2* and 4326135E for β-actin as a control). Levels are shown for three controls, parents and the proband based on the calibration curve method using an independent control. Average of duplicated experiments is shown as black bars with the standard error of means. The significant decreased expression of *DARS2* mRNA in the proband was recognized compared to that in three controls ($p < 0.001$, one-way analysis of variance with Bonferroni's multiple comparison test). (**f**) Mitochondrial aspartyl-tRNA synthetase (MtAspRS) protein is expressed in normal control and father as a carrier (fainter), but only weakly recognized in the proband. Cyclooxygenase IV was used as a loading control for the mitochondrial fraction.

Table 1. MRI criteria for LBSL and clinical features of patients

Diagnostic criteria	Case 1	Case 2	Case 3
Major criteria			
Signal abnormalities in			
1. the cerebral white matter, either inhomogeneous and spotty or homogeneous and confluent, sparing the U-fibers	±[a]	±[a]	±[a]
2. the dorsal columns and lateral corticospinal tracts of the spinal cord. (visualization of such abnormalities in the cervical spinal cord suffices)	+	n.e.[b]	n.e.
3. the pyramids of the medulla oblongata	+	+	+
Supportive criteria			
Signal abnormalities in			
1. the splenium of the corpus callosum	+	+	+
2. the posterior limb of the internal capsule	+	+	+
3. the medial lemniscus in the brain stem	+	+	+
4. the superior cerebellar peduncles	+	+	+
5. the inferior cerebellar peduncles	+	n.e.	n.e.
6. the intraparenchymal part of the trigeminal nerve	−	n.e.	n.e.
7. the mesencephalic trigeminal tracts	+	n.e.	n.e.
8. the anterior spinocerebellar tracts in the medulla	+	n.e.	n.e.
9. the cerebellar white matter with subcortical preponderance	−	−	−
Elevated lactate of abnormal cerebral white matter (MRS)	+	Not performed	+

LBSL, leukoencephalopathy with brain stem and spinal cord involvement, and lactate elevation; MRI, magnetic resonance imaging; MRS, magnetic resonance spectroscopy.
[a]Homogeneous and confluent abnormal high intensity was observed, but sparing the U-fibers was unclear because of the strenuous pathological change in the white matter.
[b]n.e., not evaluated as MRI images were unavailable.

(unidentified) modifier effect in the family and (ii) this particular homozygous mutation caused the severe variant because of the substantially decreased normal protein level, although it is not full proof.

Interestingly, affected allele frequency varies, depending on the ethnicity. For example, *DARS2* mutations are the most common causes of childhood onset leukoencephalopathy in Finland, because of high carrier frequency (1:95 for the c.228-20_21delTTinsC and 1:380 for the c.492+2T>C) (4). Thus, further analysis of the *DARS2* gene in LBSL as well as childhood-to-adult onset leukoencephalopathy of unknown cause in different populations would lead us to fully understand phenotypes of the *DARS2* abnormalities.

Acknowledgements

We thank all the patients and their families for participating in this work. We also thank Ms. Y. Yamashita for her technical assistance. This work was supported by Research Grants from the Ministry of Health, Labour and Welfare (N. M., H. S., and N. M.), the Japan Science and Technology Agency (N. M.), Grant-in-Aid for Scientific Research from Japan Society for the Promotion of Science (N. M.), Grant-in-Aid for Young Scientist from Japan Society for the Promotion of Science (N. M. and H. S.), Grant for 2010 Strategic Research Promotion of Yokohama City University (N. M.), Research Grants from the Japan Epilepsy Research Foundation (H. S.), and Research Grant from Naito Foundation (N. M.), the Takeda Science Foundation (N. M. and N. M.), the Yokohama Foundation for Advancement of Medical Science (N. M.), and the Hayashi Memorial Foundation for Female Natural Scientists (N. M.).

N Miyake[a]
S Yamashita[b]
K Kurosawa[c]
S Miyatake[a]
Y Tsurusaki[a]
H Doi[a]
H Saitsu[a]
N Matsumoto[a]
[a]Department of Human Genetics, Yokohama City University Graduate School of Medicine, Yokohama, Japan,
[b]Division of Child Neurology, and
[c]Division of Medical Genetics, Kanagawa Children's Medical Center, Yokohama, Japan

References

1. van der Knaap MS, van der Voorn P, Barkhof F et al. A new leukoencephalopathy with brainstem and spinal cord involvement and high lactate. Ann Neurol 2003: 53: 252–258.
2. Scheper GC, van der Klok T, van Andel RJ et al. Mitochondrial aspartyl-tRNA synthetase deficiency causes leukoencephalopathy with brain stem and spinal cord involvement and lactate elevation. Nat Genet 2007: 39: 534–539.
3. Uluc K, Baskan O, Yildirim KA et al. Leukoencephalopathy with brain stem and spinal cord involvement and high lactate:

a genetically proven case with distinct MRI findings. J Neurol Sci 2008: 273: 118–122.
4. Isohanni P, Linnankivi T, Buzkova J et al. *DARS2* mutations in mitochondrial leucoencephalopathy and multiple sclerosis. J Med Genet 2010: 47: 66–70.
5. Lin J, Faria EC, Da Rocha AJ et al. Leukoencephalopathy with brainstem and spinal cord involvement and normal lactate: a new mutation in the *DARS2* gene. J Child Neurol 2010: 25: 1425–1428.
6. Miyake N, Kosho T, Mizumoto S et al. Loss-of-function mutations of *CHST14* in a new type of Ehlers-Danlos syndrome. Hum Mutat 2010: 31: 966–974.

Correspondence:
Noriko Miyake, MD, PhD
Department of Human Genetics
Yokohama City University Graduate School of Medicine
3-9 Fukuura
Kanazawa-ku
236-0004 Yokohama
Japan
Tel.: +81 45 787 2606
Fax: +81 45 786 5219
e-mail: nmiyake@yokohama-cu.ac.jp